Contribution from the Departments of Chemistry, Tianjin Normal University, Tianjin, People's Republic of China, and McMaster University, Hamilton, Ontario L8S 4M1, Canada

Structure and Bonding in Sulfur–Nitrogen Compounds

TING-HUA TANG,*[1a] R. F. W. BADER,*[1b] and P. J. MacDOUGALL[1b]

Received July 24, 1984

Molecular structures (the networks of bonds) and molecular geometries are determined in SCF calculations for S_2N_2, S_4^{2+}, $S_4N_4^{2+}$, S_4N_4, and H_2S_2 (with the STO-3G and 6-21G* basis sets) and for $S_6N_4^{2+}$, S_8, S_8^{2+}, and S_8^{4+} (with the STO-3G basis set). The chemical bonds are defined and classified in terms of the properties of the *total* charge distribution. In particular, molecular structures are determined by finding those pairs of nuclei linked by lines along which the charge density is a maximum with respect to any neighboring line, i.e., those nuclei linked by a bond path. In S_4N_4, for example, each S nucleus is linked to two N nuclei and to another S nucleus, while each N nucleus is linked to two S nuclei. The regions where electronic charge is locally concentrated and depleted within the valence shell of each atom are also determined. This information provides a charge density analogue of the Lewis electron pair model and determines the sites of electrophilic and nucleophilic attack within a molecule. In S_4N_4, for example, the valence shell of each S atom exhibits one nonbonded and three bonded charge concentrations, while each N atom exhibits two bonded and two nonbonded charge concentrations. The relatively long S–S bonds in S_4N_4 and $S_6N_4^{2+}$ and the cross-ring bonds found to be present in S_8^{2+} and S_8^{4+} exhibit the characteristics of closed-shell interactions as opposed to the other S–S and the S–N bonds in these molecules, which exhibit characteristics typical of shared interactions.

Introduction

Sulfur–nitrogen compounds exhibit interesting physical,[2] structural,[3] and bonding properties.[4] The synthesis of $S_4N_4^{2+}$ in 1977 coupled with the demonstration of its planar geometrical structure[5] strengthened earlier theoretical considerations of Gleiter[4] regarding the electronic structures of S–N compounds.

The molecular structure of a system, i.e., the network of chemical bonds, is unambiguously determined by the form of its electronic charge distribution.[6,7] The same properties of the charge distribution, coupled with quantum-mechanical considerations,[8,9] provide a definition of an atom in a molecule and enable one to determine its average properties. This theory of molecular structure is used to define the structures of S_2N_2, S_4N_4, $S_4N_4^{2+}$, and $S_6N_4^{2+}$. The characterization of bonds as provided by this theory[10,11] shows that the S–S bonds present in S_4N_4 and $S_6N_4^{2+}$ are not of the normal shared or covalent type. Evidence of a corresponding long S–S bond in S_8^{2+} has been found,[12] and such bonds should also be present in S_8^{4+}, an isoelectronic analogue of S_4N_4. For this reason the theory has been applied as well to the systems S_8, S_8^{2+}, and S_8^{4+}, and also to S_4^{2+}, the sulfur analogue of S_2N_2. The molecule H_2S is also included to provide a further example of an S–S bond.

The equilibrium geometries, energies, and electronic charge distributions of all the molecules were determined in SCF calculations with the STO-3G basis set. Calculations at these geometries were repeated by using the STO-3G* basis (d-type basis functions on S)[13] for S_2N_2, S_4N_4, $S_4N_4^{2+}$, and H_2S_2. Separate geometry optimizations were also made for H_2S_2, S_4^{2+}, S_2N_2, and $S_4N_4^{2+}$ with use of the 6-21G* basis set.[14] A calculation was also done for S_4N_4 with this basis set at the experimental geometry. The geometrical parameters and E(SCF) values are given in Table I for all the calculations. In general, the theoretically determined geometries are in good agreement with the known experimental results. An STO-3G geometry and energy have been previously reported for S_2N_2,[15] giving a shorter S–N bond length (3.203 au) and a higher energy (E(SCF) = −893.6116 au).

Molecular Structures of S_nN_n and S_n

Molecular structure, as distinct from molecular geometry, is determined by the topological properties of the system's charge distribution. The observation of interatomic separations smaller than the corresponding van der Waals contact distances, such as occurs in a number of the molecules studied here, does not enable one to establish whether or not the atoms are bonded to one another. The definition of molecular structure follows directly from the identification of an atom as a quantum subsystem—one whose average properties are defined by and satisfy the theorems of quantum mechanics.[6,9] The quantum condition defining the subsystem or atom is simply stated: the surface bounding the atom shall not be crossed by any gradient vectors of the charge density $\rho(\mathbf{r})$. This condition of zero flux in $\nabla\rho(\mathbf{r})$ through the atomic surface may be stated as

$$\nabla\rho(\mathbf{r})\cdot\mathbf{n}(\mathbf{r}) = 0 \qquad (1)$$

for every point on the surface of the atom, where $\mathbf{n}(\mathbf{r})$ is the unit vector normal to the surface at $\mathbf{r}$. The vector $\nabla\rho$ points in the direction of maximum increase in ρ. A gradient path is generated by following the path traced out by a succession of such vectors starting at some initial point. By displaying the gradient vector field of $\rho(\mathbf{r})$, the *collection* of paths traced out by the gradient vectors of $\rho(\mathbf{r})$, one finds that a molecular charge distribution is partitioned into atoms in a natural way by the quantum condition eq 1 and that this identification of the atom with a quantum subsystem leads to a definition of molecular structure.

The single most striking observation regarding the form of ρ is that it exhibits local maxima only at the positions of nuclei. A local maximum means that electronic charge is most dense at the position of a nucleus and becomes less dense as one moves away from the nucleus in *any* direction. Thus in a diagram that portrays ρ in a given plane (Figure 1a), ρ will exhibit a maximum at a nuclear position for any plane containing that nucleus. Correspondingly, in a display of the gradient vector field of ρ, all the gradient paths in the vicinity of a nucleus will terminate at the nucleus. A nucleus is said to behave as an *attractor* in the gradient vector field and *nuclei are the only attractors in the field* $\nabla\rho$. The

(1) (a) Tianjin Normal University. (b) McMaster University.
(2) Green, R. L.; Grantand, P. M.; Street, G. B. *Phys. Rev. Lett.* **1975**, *34*, 577. Green, R. L.; Street, G. B.; Suter, L. J. *Phys. Rev. Lett.* **1975**, *35*, 1799.
(3) Lu, C.-S.; Donohue, J. *J. Am. Chem. Soc.* **1944**, *66*, 818. Sharma, B. D.; Donohue, J. *Acta Crystallogr.* **1963**, *16*, 891.
(4) Gleiter, R. *J. Chem. Soc. A* **1970**, 3174. Gleiter, R. *Angew. Chem., Int. Ed. Engl.* **1981**, *20*, 444.
(5) Gillespie, R. J.; Slim, D. R.; Tyrer, J. D. *J. Chem. Soc., Chem. Commun.* **1977**, 253. Gillespie, R. J.; Kent, J. D.; Sawyer, J. R.; Slim, D. R.; Tyrer, J. D. *Inorg. Chem.* **1981**, *20*, 3799.
(6) Bader, R. F. W.; Nguyen-Dang, T. T.; Tal, Y. *Rep. Prog. Phys.* **1981**, *44*, 893.
(7) Bader, R. F. W.; Nguyen-Dang, T. T.; Tal, Y. *J. Chem. Phys.* **1979**, *70*, 4316.
(8) Bader, R. F. W. *J. Chem. Phys.* **1980**, *73*, 2871.
(9) Bader, R. F. W.; Nguyen-Dang, T. T. *Adv. Quantum Chem.* **1981**, *14*, 63.
(10) Bader, R. F. W.; MacDougall, P. J.; Lau, C. D. H. *J. Am. Chem. Soc.* **1984**, *106*, 1594.
(11) Bader, R. F. W.; Essén, H. *J. Chem. Phys.* **1984**, *80*, 1943.
(12) Davies, C. G.; Gillespie, R. J.; Park, J. J.; Passmore, J. *Inorg. Chem.* **1971**, *10*, 2781.
(13) Collins, J. B.; Schleyer, P. R.; Binkley, J. S.; Pople, J. A. *J. Chem. Phys.* **1976**, *64*, 5142.
(14) Binkley, J. S.; Pople, J. A.; Hehre, W. J. *J. Am. Chem. Soc.* **1980**, *102*, 939. Gordon, M. S.; Binkely, J. S.; Pople, J. A.; Pietro, W. J.; Hehre, W. J. *J. Am. Chem. Soc.* **1982**, *104*, 2797.
(15) Kertész, M.; Suhai, S.; Azman, A.; Kocjan, D.; Kiss, Á. I. *Chem. Phys. Lett.* **1976**, *44*, 53.

0020-1669/85/1324-2047$01.50/0

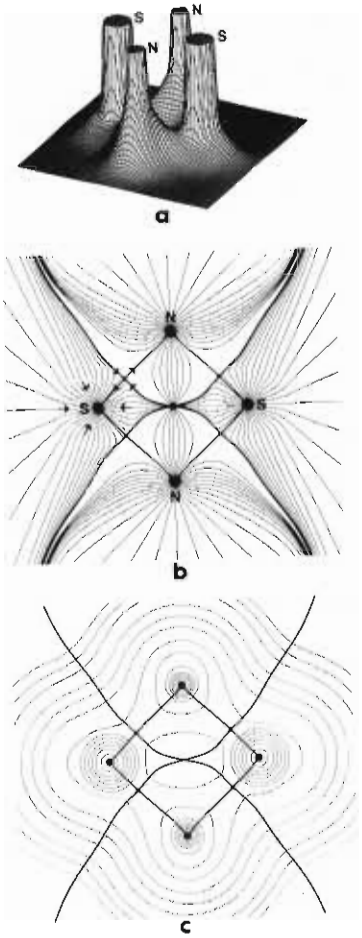

Figure 1. Displays of the charge density ρ and its gradient vector field for the plane of the nuclei in S_2N_2 (6-21G* calculation). In (a) ρ is plotted in the third dimension. Note the asymmetry in the distribution along an S–N bond. While the bond saddle point approaches the S core, there is a shoulder of nonbonded valence density on S. In (b) trajectories of $\nabla\rho$ are displayed. All trajectories terminate at nuclei except for the pairs that in this plane *terminate* at each bond critical point and define the boundaries of the atoms. The pairs of trajectories that *originate* at each bond cp and terminate at neighboring nuclei define the bond path. In (c) the bond paths and the boundaries of the atoms are shown superposed on a contour map of ρ.

region of three-dimensional space traversed by all gradient paths that terminate at a given attractor defines the *basin* of the attractor. Thus this single, dominant observation regarding the form of ρ yields a complete partitioning of the real space of a molecular system. The system is partitioned into a set of basins, and each basin contains a single attractor, i.e., nucleus. This is illustrated in Figure 1b. Since every gradient path in a given basin terminates at the attractor of that basin, it necessarily follows that no trajectories of $\nabla\rho$ will cross the surface separating neighboring basins—this partitioning satisfies the zero flux surface condition of quantum mechanics. From this point on, *each attractor and its associated basin will be called an atom.*

By studying the behavior of the remaining gradient paths, those that originate and terminate at critical points in ρ—points where $\nabla\rho(\mathbf{r}) = 0$—we can define an interatomic surface and show that it satisfies the quantum subsystem condition, eq 1.

Reference to Figures 1 and 2 illustrates that ρ exhibits a saddle point between some but not all pairs of nuclei in a molecule—it does between adjacent S and N nuclei in S_2N_2 (Figure 1) and in S_4N_4 (Figure 2) for example, but not between the N nuclei in S_4N_4. If ρ retains this form when viewed in every plane containing the internuclear axis, then it contains a critical point at which ρ is a minimum with respect to one direction (along the line of the nuclei) and a maximum with respect to all directions perpendicular to this line. This is true of the saddle points appearing in Figures 1 and 2. One notes that the presence of such a critical point [called

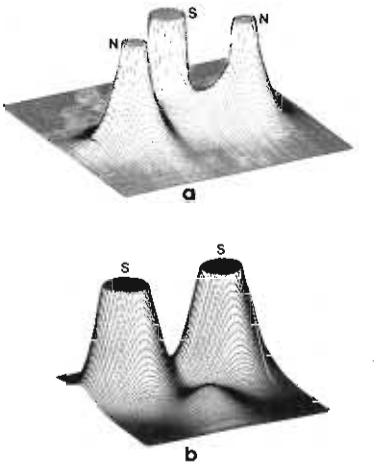

Figure 2. Displays of ρ for S_4N_4 (6-21G*). In (a) ρ is displayed in the third dimension for a plane containing one S and two N nuclei. In (b) ρ is displayed for a plane containing two S nuclei and bisecting the line linking the second two S nuclei. Thus this single diagram gives two views of the S–S bond critical point: for the in-plane S atoms ρ exhibits one negative and one positive curvature and ρ appears as a saddle; for the out-of-plane S atoms ρ exhibits two negative curvatures (the interatomic surface) and ρ appears as a maximum. The charge density also exhibits a local minimum in this plane, at the position of the cage critical point. This minimum in ρ will appear in any plane containing this critical point.

a (3,−1) cp since it has three curvatures, one positive and two negative, $+1 - 1 - 1 = -1$] between a pair of nuclei indicates that electronic charge *is accumulated between them.* If one displays ρ in a plane perpendicular to the internuclear axis, then ρ exhibits a maximum at the position of a (3,−1) cp (Figure 2b). Since ρ is a maximum in two dimensions at such a critical point, a set of gradient paths will terminate at this point and define a surface—the interatomic surface separating the basins of two *neighboring atoms.* Thus, a (3,−1) cp is found between every pair of neighboring atoms. The basin of each atom is bounded by one or more interatomic surfaces as generated by the sets of trajectories of $\nabla\rho$ that terminate at the corresponding (3,−1) critical points. Surfaces defined by trajectories of $\nabla\rho$ are necessarily surfaces of zero flux as illustrated in Figure 1.

The quantum condition governing the definition of a subsystem is fulfilled in a natural way by the form of a molecular charge distribution, the condition yielding a partitioning of space into distinct nonoverlapping regions, each region containing a single nucleus. The same properties of the gradient vector field of ρ that yield the definition of an atom as a quantum subsystem contain the necessary information for the definition of molecular structure.

The charge density in an interatomic surface is a maximum at the (3,−1) cp. The value of ρ is also a minimum at this same point along a line perpendicular to the surface at the critical point that links the two neighboring nuclei. This line is defined by the two and only two gradient paths that originate at a (3,−1) cp. Each terminates at one of the neighboring nuclei. The presence of these two gradient paths indicates the existence of a line linking the nuclei along which the charge density is a maximum with respect to any neighboring line. These lines are called *atomic interaction lines* because they exist only between atoms that share a common surface. The network of such lines is called a *molecular graph.* If the nuclei are linked by interaction lines so as to form a ring, then a critical point called a ring cp is found in the interior of the ring. The charge density is a minimum at this point in the ring surface. The S_2N_2 molecule (Figure 1) is a ring structure, and the minimum in ρ at the center of the ring surface is evident in the display of ρ shown in this figure. If the nuclei are linked so as to enclose the interior of the molecule with ring surfaces, then another and final kind of critical point is found in the interior of the resulting cage. The charge density is a local minimum at a cage critical point. This is exemplified by the display of ρ for the S_4N_4 molecule in Figure 2b. The interior of this molecule is bounded by the surfaces of four five-membered rings, and one

Table I. Calculated Geometries and Energies[i]

molecule	geom parameter[k]	exptl value	STO-3G value	6-21G* value	*E*(RHF) STO-3G	*E*(RHF) STO-3G*	*E*(RHF) 6-21G*
S_2N_2	*R*(SN)	1.65[a]	1.70	1.62	−893.67558	−893.93340	−903.67455
	∠NSN	90.0	86.6	89.7			
S_4^{2+}	*R*(SS)	2.01[b]	2.06	1.99	−1572.01168		−1589.11965
	∠SSS	90.0	90.0	90.0			
$S_4N_4^{2+}$	*R*(SN)	1.56[c]	1.61	1.54	−1786.74987	−1787.41447	−1806.60898
	∠SNS	151.2	157.5	159.2			
$S_6N_4^{2+}$	*R*(S*N)	1.61[d]	1.66		−2573.17399		
	R(SN)	1.57	1.61				
	R(S*S*)	2.14	2.19				
	R(S*S**)	3.03	3.05				
	∠NSS	97.0	96.3				
	∠SNS	107.8	105.2				
	∠NSN	119.1	121.1				
	α[j]	111.7	109.9				
S_4N_4	*R*(S*N)	1.62[e]	1.69	1.62	−1787.27847	−1787.93196	−1807.19601
	R(S*S*)	2.58	2.53	2.58			
	∠NSN	105.0	104.5	105.4			
H_2S_2	*R*(HS)	1.35[f]	1.34	1.33	−787.48870	−787.64529	−796.16305
	R(SS)	2.06	2.09	2.06			
	∠HSS	92.0	92.0	99.0			
	∠HSSH(dihedral)	90.5	94.0	89.9			
S_8	*R*(SS)	2.04[g]	2.07		−3145.46178		
	∠SSS	104.0	105.0				
S_8^{2+}	*R*(SS)	2.04[h]	2.09		−3144.86638		
	R(SS*)	2.04	2.06				
	R(S*S*)	2.86	2.22				
	∠SSS	93.0	93.6				
	∠SS*S	102.0	104.2				
S_8^{4+}	*R*(SS*)		2.08		−3143.42027		
	R(S*S*)		2.47				
	∠SS*S		105.0				

[a] MacDiarmid, A. G.; Mikulski, C. M.; Russo, P. J.; Saran, M. S.; Garito, A. F.; Heeger, A. J. *J. Chem. Soc., Chem. Commun.* **1975**, 476. [b] Passmore, J.; Sutherland, G.; White, P. S. *J. Chem. Soc., Chem. Commun.* **1980**, 330. [c] Gillispie, R. J.; Kent, J. P.; Sawyer, J. F.; Slim, D. R.; Tyrer, J. D. *Inorg. Chem.* **1981**, *20*, 3799. [d] Gillespie, R. J.; Kent, J. P.; Sawyer, J. F. *Inorg. Chem.* **1981**, *20*, 3784. [e] Sharma, B. D.; Donohue, J. *Acta Crystallogr.* **1963**, *16*, 891. [f] Winnewisser, M.; Haase, J. *Z. Naturforsch., A: Astrophys., Phys., Phys. Chem.* **1968**, *A23*, 56. [g] Caron, A.; Donohue, J. *Acta Crystallogr.* **1965**, *18*, 562. [h] Gillespie, R. J.; Passmore, J.; Ummat, P. K.; Vaidya, O. C. *Inorg. Chem.* **1971**, *10*, 1327. [i] Bond distances are in angstroms, angles in degrees, and RHF energies in atomi units, 1 au = 627.51 kcal/mol. [j] α = dihedral angle between five- and four-membered rings. [k] S* is the sulfur of a bridging bond; S*S** is the long bridge in $S_6N_4^{2+}$.

view of the local minimum attained by ρ at the cage critical point is illustrated. Thus, the topology of ρ is such that its critical points allow for the definition of atoms and the network of lines that show how the atoms are linked to one another. They further indicate the presence of rings or cages in the structures so defined. In a bound system an atomic interaction line is called a *bond path*. The existence of a bond path is both a *necessary* and *sufficient* condition for the existence of a bond.[11]

The network of bond paths is found to coincide with the network of chemical bonds that are assigned to define a chemical structure. In general, it is found that the same molecular graph is obtained over some open region of nuclear configuration space. That is, the same nuclei remain linked by the same number of bond paths as the nuclei undergo their vibrational motions. A molecular graph with these properties is said to represent a stable structure.[6]

The molecular structures for the molecules considered here are illustrated by representative molecular graphs in Figure 3. The position of each (3,−1) or bond critical point in a charge distribution is indicated by a black dot. The presence of such a critical point indicates the existence of both a bond path and an interatomic surface between the bonded pair of atoms (Figure 1c). The critical point of an S–N bond is not equidistant from the nuclei but closer to the former nucleus, indicative of a transfer of charge from S to N. Correspondingly, the displays of ρ given in Figures 1a and 2a show that the valence charge density is assymmetrically disposed in favor of the nitrogen atom. A S–N bond path can be curved and not coincident with the corresponding internuclear axis. Most of the curvature in these bonds occurs close to the nuclei, and hence the bond path angle can be noticeably different from the geometric angle. The limiting value of the NSN bond path angle at a sulfur nucleus in S_4N_4 (6-21G* calculation) for example, is 99.6° compared to a bond angle of 105.40°, indicating

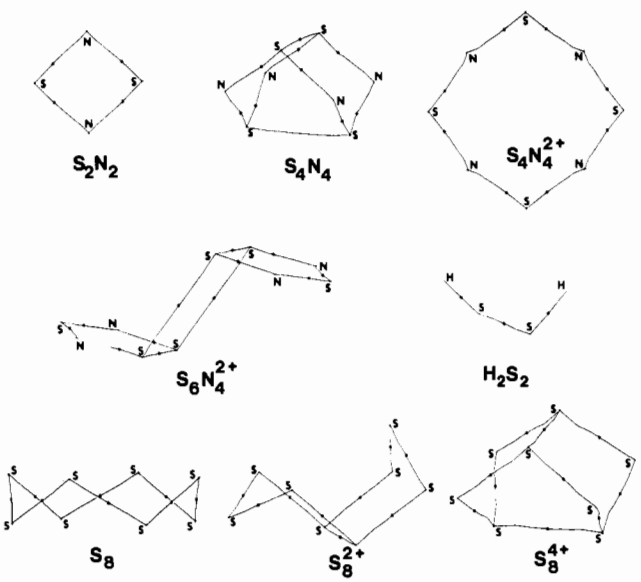

Figure 3. Molecular graphs representative of the molecular structures. These are planar projections of the bond paths defined by the pairs of trajectories of $\nabla\rho$ which originate at each bond cp (denoted by a black dot).

that the "bond strain" in such a five-membered ring is less than suggested by the geometry of the system. The other major differences between geometric and bond path angles are found for the SNS angles in S_2N_2 and $S_4N_4^{2+}$: in S_2N_2 an SNS bond path angle of 79.1° (6-21G* calculation) is 11.2° smaller than the

Table II. Properties of S–N and S–S Bonds[a]

molecule	bond[b]	STO-3G			6-21G*		
		ρ_b	$\nabla^2\rho(\mathbf{r}_c)$	ϵ	ρ_b	$\nabla^2\rho(\mathbf{r}_c)$	ϵ
S_2N_2	S–N	0.183	+0.175	1.432	0.236	+0.285	0.572
S_4^{2+}	S–S	0.128	−0.072	0.307	0.183	−0.326	0.274
$S_4N_4^{2+}$	S–N	0.167	+0.823	1.340	0.234	+0.646	0.383
$S_6N_4^{2+}$	S*–N	0.171	+0.551	1.800			
	S–N	0.184	+0.710	0.801			
	S*–S*	0.102	+0.022	0.200			
	S*–S**	0.017	+0.072	0.000			
S_4N_4	S*–N	0.190	−0.205	0.143	0.236	−0.223	0.118
	S*–S*	0.055	+0.124	0.053	0.062	+0.052	0.064
H_2S_2	S–S	0.120	−0.066	0.019	0.149	−0.195	0.002
S_8	S–S	0.125	−0.058	0.037			
S_8^{2+}	S–S	0.118	−0.021				
	S–S*	0.119	−0.042	0.089			
	S*–S*	0.060	+0.080	0.072			
S_8^{4+}	S–S*	0.118	−0.024	0.263			
	S*–S*	0.045	+0.047	0.075			

[a] All quantities are in atomic units: for ρ, 1 au = e/a_0^3 = 6.748 e/Å^3; for $\nabla^2\rho$, 1 au = e/a_0^5 = 24.10 e/Å^5. [b] S* is the sulfur of a bridging bond (Figure 3); S*S** is the long bridge in $S_6N_4^{2+}$.

geometric value while in $S_4N_4^{2+}$ the corresponding values are 148.0 and 11.2°.

The value of ρ at a bond critical point, denoted by ρ_b, provides a relative measure of bond strength for a given type of bond.[16,17] These values are listed in Table II and serve as an introductory guide to the nature of the bonding in these molecules. A full discussion of the bonding is given in the following section. A discussion and summary of each structure is given below. The individual structure assignments are found to be independent of basis set.

The S_2N_2 molecule is a ring structure. The minimum value attained by $\rho(\mathbf{r})$ in the ring surface at the position of the ring critical point is 0.090 au compared to its minimum value in the circumference of the ring, the value of ρ_b for an S–N bond, 0.236 au.

The S_4N_4 molecule is a cage structure, its interior being bounded by four S–N–S–N–S rings. There are no (3,−1) critical points linking the nitrogens in this molecule, and hence there are no N–N bonds. The charge density attains its minimum value in the interior of the molecule (6-21G*) at the cage critical point where ρ = 0.0147 au. Its value at a ring critical point is 0.0207 au. While the S–S interatomic separation in this molecule is considerably greater than that found in H_2S_2, the S atoms of S_4N_4 are linked by lines along which ρ is a maximum with respect to any neighboring lines. There are S–S bonds in this molecule, but the value of ρ_b is considerably less than that for S–S bonds in H_2S_2 or S_8.

Salts of the $S_4N_4^{2+}$ cation have been recently prepared and their crystal structures determined.[18] This cation is in general found to have the form of a planar ring with D_{4h} symmetry and equal bond lengths. The calculated S–N bond length is in good agreement with the experimental value. The calculated charge distributions predict a ring structure for this molecule with a single ring critical point at the center of the ring surface where $\rho(\mathbf{r})$ = 0.0013 au (STO-3G* basis). The distance between next nearest sulfur atoms, ~3.0 Å, is below their van der Waals contact distance of 3.7 Å, and the possibility of direct but weak bonding between such pairs of atoms has been suggested.[18] This possibility is not borne out by the topological properties exhibited by the charge density of $S_4N_4^{2+}$.

The $S_3N_2^+$ radical cation may exist as a monomer or as the dimer $S_6N_4^{2+}$.[18,19] The structure of the dimer consists of two identical planar $S_3N_2^+$ cations linked to each other in a chair conformation by two long S–S bonds (cf. Figure 3). This structure is confirmed by the topological properties ρ. The ring formed by the long S–S bonds possesses a ring critical point at which ρ = 0.004 au.

On the basis of X-ray diffraction studies, the S_8^{2+} cation is a folded ring having an exo–endo conformation. These studies suggested the presence of a cross-ring S–S bond to yield a bicyclic structure.[12] This structure is again confirmed by the form exhibited by $\rho(\mathbf{r})$. There is a (3,−1) critical point at the center of the structure between a pair of sulfur atoms, and these atoms are linked by a bond path (cf. Figure 3). As required by this structure, a ring critical point is found at the center of each of the resulting five-membered rings at which ρ = 0.010 au.

The hypothetical S_8^{4+} ion is isoelectronic with S_4N_4 and is predicted to have the same endo–endo conformation and structure. The values of ρ_b for the long S–S bonds in S_8^{4+} and S_4N_4 are similar as is that of the single long cross-ring bond in S_8^{2+}. The crown-shaped S_8 molecule has an exo–exo conformation with no cross-ring bonds. A single ring critical point is found with ρ = 0.0004 au. The exo–endo conformation of the S_8^{2+} molecule is thus intermediate between the exo–exo and endo–endo conformations, respectively, of S_8 and S_8^{4+}. Beginning with S_8, each removal of a pair of electrons results in the formation of a cross-ring bond and the eventual transformation of the ring structure of S_8 into the cage structure of S_8^{4+}.

The analysis of the bonding in these molecules presented in the following sections shows that the long S–S bonds found in S_4N_4, $S_6N_4^{2+}$, S_8^{2+}, and S_8^{4+} are not only weaker than normal S–S bonds, as suggested by the relatively low values of ρ_b, but also are of a different nature.

Bonding and Reactivity

The charge density $\rho(\mathbf{r})$ exhibits local maxima only at the positions of nuclei. Thus, discussions of bonding and reactivity based upon models that invoke the existence of localized electron pairs, bonded and nonbonded, cannot be related to the form of the charge density itself. The model of localized electron pairs is, however, evident in the form of a function related to $\rho(\mathbf{r})$, its Laplacian distribution.[10] The Laplacian of a scalar function in three dimensions such as ρ is simply the sum of the three principal curvatures of the function at each point in space:

$$\nabla^2\rho(\mathbf{r}) = \frac{\partial^2\rho}{\partial x^2} + \frac{\partial^2\rho}{\partial y^2} + \frac{\partial^2\rho}{\partial z^2} \qquad (2)$$

When $\nabla^2\rho(\mathbf{r}) < 0$, then the value of the charge density at the point $\mathbf{r}$ is greater than the value of $\rho(\mathbf{r})$ averaged over all neighboring points in space, and when $\nabla^2\rho(\mathbf{r}) > 0$, $\rho(\mathbf{r})$ is less than this averaged value. Thus a maximum in $-\nabla^2\rho(\mathbf{r})$ menas that electronic charge is locally *concentrated* in that region of space even though the charge density itself exhibits no corresponding maximum. One

(16) Bader, R. F. W.; Tang, T. H.; Tal, Y.; Biegler-König, F. W. *J. Am. Chem. Soc.* **1982**, *104*, 940.
(17) Bader, R. F. W.; Slee, T. S.; Cremer, D.; Kraka, E. *J. Am. Chem. Soc.* **1983**, *105*, 5061.
(18) Gillespie, R. J.; Kent, J. P.; Sawyer, J. F. *Inorg. Chem.* **1981**, *20*, 3784.
(19) Banister, A. J.; Clarke, H. G.; Rayment, I.; Shearer, H. M. M. *Inorg. Nucl. Chem. Lett.* **1974**, *10*, 647. Krebs, B.; Henken, G.; Pohl, S.; Roesky, H. W. *Chem. Ber.* **1980**, *113*, 226.

may think of $\nabla^2\rho$ as providing a measure of the extent to which the charge density is locally compressed or expanded. This property of ρ must be distinguished from local maxima and minima in $\rho(\mathbf{r})$ itself.

The Laplacian of $\rho(\mathbf{r})$ recovers the shell structure of an atom by displaying a corresponding number of pairs of shells of charge concentration and charge depletion.[10] On bonding, the uniform outer or valence shell charge concentration of a free atom is distorted so as to form "lumps" and "holes" in this shell. The maxima in $-\nabla^2\rho$ recover in a most satisfying way the "lumps" in a molecular charge distribution as anticipated in terms of the Lewis electron pair model or as surmised to exist in Gillespie's VSEPR model of molecular geometry.[20] These local concentrations of charge determine the sites of electrophilic attack. The points where $-\nabla^2\rho$ attains its minimum values locate the "holes" in the valence shell charge concentration. These holes, since they give direct access to the core of the atom, are the sites of nucleophilic attack.

The Laplacian of ρ plays a dominant role in the theory of atoms in molecules. The quantum condition for the definition of an atom, eq 1, when integrated over the surface of an atom Ω yields a constraint on the atomic average of the Laplacian of ρ:

$$\oint_S \mathrm{d}S\ \nabla\rho\cdot\mathbf{n} = \int_\Omega \nabla^2\rho\ \mathrm{d}\tau = 0 \qquad (3)$$

While there is no constraint on the amount of electronic charge contained within the boundaries of an atom, there is a constraint on the relative extents of concentration and depletion of charge. According to eq 3, if charge is concentrated in some regions of an atom, it must be depleted to a corresponding extent in other regions. This property is common to all atoms, free or bound. The Lagrangian approach to quantum mechanics yields relationships between local values of mechanical properties as well as between their average values. In particular the local expression for the virial theorem is

$$(\hbar^2/4m)\nabla^2\rho(\mathbf{r}) = \mathcal{V}(\mathbf{r}) + 2G(\mathbf{r}) \qquad (4)$$

where $\mathcal{V}(\mathbf{r})$ and $G(\mathbf{r})$ are the potential and kinetic energy densities, respectively. Since the integral of $\nabla^2\rho$ vanishes over an atom as well as over the total system, one obtains the virial theorem $\mathcal{V}(\Omega) + 2T(\Omega) = 0$, in both cases. Since $G(\mathbf{r}) > 0$, eq 4 demonstrates that the lowering of the potential energy dominates the energy in regions of space where electronic charge is concentrated, i.e., where $\nabla^2\rho < 0$.[11]

The charge density is a maximum in an interatomic surface at the (3,−1) or bond critical point. The two curvatures of ρ perpendicular to the bond path at the critical point $\mathbf{r}_c$ are, therefore, negative and charge is locally concentrated in the interatomic surface at $\mathbf{r}_c$. Since $\rho(\mathbf{r})$ is a minimum at $\mathbf{r}_c$ along the bond path, the third or parallel curvature of ρ at a bond critical point is positive. Charge is locally depleted at $\mathbf{r}_c$ with respect to neighboring points on the bond path. Thus, the formation of an interatomic surface and a chemical bond is a result of a competition between the perpendicular contractions of $\rho(\mathbf{r})$ leading to a concentration or compression of electronic charge along the bond path and the parallel expansion of ρ leading to a depletion of charge in the interatomic surface and to its separate concentration in the basins of the neighboring nuclei. When $\nabla^2\rho < 0$, the perpendicular curvatures dominate the interaction and electronic charge is concentrated along the bond path. The result is a sharing of electronic charge between the atoms as is found in covalent or polar bonds. This type of bonding is exemplified by S_4^{2+}, the all-sulfur analogue of S_2N_2. The Laplacian of ρ for this molecule is shown in Figure 4a. The atomic interactions are dominated by the perpendicular contractions in ρ, and the Laplacian is negative in the valence region of the bond path. Hence, the valence shells of charge concentration of neighboring atoms are joined together by a concentration of electronic charge. One also notes the presence of a nonbonded charge concentration, as well as two regions of charge depletion in the valence shell of each sulfur atom.

(20) Gillespie, R. J. "Molecular Geometry"; Van Nostrand-Reinhold: London, 1972.

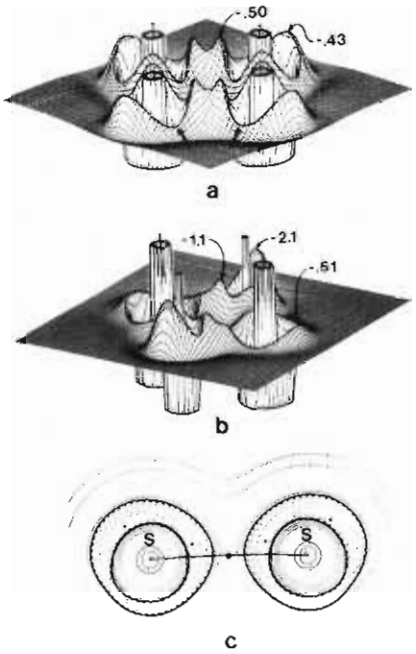

Figure 4. Displays of the negative of the Laplacian of ρ ($-\nabla^2\rho$) for (a) S_4^{2+}, (b) S_2N_2, and (c) S_4N_4. Parts a and b are not to the same scale. Instead, the numerical values of the bonded and nonbonded maxima are indicated on the diagram. Counting the peak in $-\nabla^2\rho$ at a nucleus, each S atom exhibits three alternating shells of charge concentration and charge depletion while each N atom exhibits only two such alternating shells. Each plot has a cutoff value, and the inner shell maxima and minima are not shown. The arrows in (a) indicate the positions of local minima in the valence shell charge concentrations of the S atoms. These are the preferred sites of interaction with neighboring bases in a crystal or of nucleophilic attack. Part c is a contour display of $\nabla^2\rho$ for an S–S bond in S_4N_4 showing as well the bond path and associated critical point. Dashed contours indicate negative values for $\nabla^2\rho$ and the regions of charge concentration. The small dots indicate the positions of the nonbonded and bonded maxima in the valence shell charge concentration of each S atom. Note the distinct polarization of each such shell toward the other. Unlike an S–S bond in S_4^{2+} (a), where charge is concentrated between and shared by both nuclei (a shared interaction), the charge in the S–S bond of S_4N_4 is separately localized and concentrated within the basin of each atom as is typical of a closed-shell interaction.

The S–S bonds in S_2, H_2S_2, and S_8 and the nonbridging S–S bonds in S_8^{2+} and S_8^{4+} all have $\nabla^2\rho < 0$ at the bond critical point (Table II). All exhibit a similar concentration of electronic charge linking the atoms as a result of the interactions being dominated by the contractions of ρ perpendicular to the bond path. The nuclei are bound by the shared concentration of charge. By eq 4 this concentration of charge gives rise to a lowering of the potential energy over the binding region and hence to an increase in the stability of the system.

The S–N bond is very polar. The net charge on an atom in a molecule is determined by integration of $\rho(\mathbf{r})$ over the basin of the atom to yield its average electron population followed by subtraction of this number from the nuclear charge. The net charges for the sulfur atoms in S_2N_2, S_4N_4, and $S_4N_4^{2+}$ are respectively +1.22, +1.29, and +1.95 e with use of the STO-3G* basis. A comparison of $\nabla^2\rho$ for S_4^{2+} and S_2N_2 (parts a and b of Figure 4) shows a large concentration of charge linking the respective cores in both molecules. The S–N bonds are shared interactions as are the S–S bonds. The values of ρ_b are relatively large for both molecules, but the bonded charge concentration is strongly polarized toward the nitrogen nucleus in an S–N bond. The critical point for an S–N bond falls close to the boundary where $\nabla^2\rho(\mathbf{r})$ changes sign. Hence $\nabla^2\rho(\mathbf{r})$ at the bond critical point is less than zero for S_4N_4 and greater than zero for S_2N_2.

The long S–S bonds in N_4S_4 and the ions S_8^{2+}, S_8^{4+}, and $S_6N_4^{2+}$ all have $\nabla^2\rho > 0$ over the interatomic surface (Table II) and are examples of the second limiting type of atomic interaction—interactions dominated by contractions in the charge density toward each of the nuclei as reflected in the dominance of the

positive curvature parallel to the bond path. They are called closed-shell interactions, as they typify interactions between closed-shell atoms as found in noble-gas repulsive states, ionic bonds, hydrogen bonds, and van der Walls molecules. The relative depletion of charge in the interatomic surface characteristic of these interactions is a consequence of the Pauli principle. Hence, it is not surprising to find the same characteristics to be exhibited by the third bond to a sulfur atom as the Lewis model would predict only two shared interactions.

Figure 4c shows the Laplacian of ρ for a S–S bond in N_4S_4. As is typical of "closed-shell" interactions, the regions of charge concentration and hence of dominant potential energy decrease are separately localized within the basins of the interacting atoms—there is no shared concentration of charge. Clearly such an interaction may, in general, result in a bound or unbound state depending upon the direction of polarization of each atomic charge distribution.[10,11] The Laplacian of ρ for an S–S bond in N_4S_4 shows that the valence shell charge concentration of each sulfur atom is strongly polarized toward its neighbor as required for a bonded interaction. In addition, the Laplacian of ρ indicates the presence of a nonbonded charge concentration on each sulfur atom.

In summary, a sulfur atom bearing a net positive charge, by virtue of the system being positively charged as in S_8^{2+} and S_8^{4+} or because of a transfer of charge to a neighboring nitrogen, can form three bonds. Two of the bonds result from the sharing of a relatively large concentration of charge which is accumulated between the nuclei. The third bond, a sulfur–sulfur bond, is formed as a result of the inward polarization of the valence shell charge concentrations, each of which remains separately localized on the sulfur atoms. The resulting bond is longer and weaker than one arising from a shared interaction because of the relatively small amount of charge accumulated in the interatomic surface as evidence by the small value for ρ_b.

In a bond with cylindrical symmetry the two negative curvatures of ρ at the bond critical point are of equal magnitude. However, if electronic charge is preferentially accumulated in a given plane, then the rate of falloff in ρ from its value ρ_b is less in this plane than in the one perpendicular to it and the magnitude of the corresponding curvature of ρ is smaller. If the two negative curvatures of ρ at a bond critical point are denoted by λ_1 and λ_2 with λ_2 being the curvature of smallest magnitude, the quantity $\epsilon = \lambda_1/\lambda_2 - 1$, the ellipticity of the bond, provides a measure of the extent to which electronic charge is preferentially accumulated in a given plane.[17] Thus, for example, the ellipticity of the C–C bond in ethane is zero, greater than zero for benzene, and larger still for ethylene with the curvature of smallest magnitude being directed perpendicular to the plane of the nuclei in the last two molecules. Thus the ellipticity of a bond provides a relative measure of the "π character" of a bond. The ellipticities ϵ are given in Table II for the STO-3G and 6-21G* basis sets. The minimal STO-3G basis set exaggerates the spread in the values of ϵ, but the complete survey of values obtained for this set illustrates the primary result also exhibited by the more reliable values obtained from the 6-21G* set—that the values of ϵ are large for bonds in those molecules (S_2N_2, S_4^{2+}, $S_4N_4^{2+}$, $S_6N_4^{2+}$) which are anticipated to exhibit π character and relatively small for the bonds in the remaining molecules. Only the results obtained with the 6-21G* set are discussed in detail.

In the orbital model of electronic structure the molecules S_4^{2+} and S_2N_2 possess 6 π electrons and $S_4N_4^{2+}$ possesses 10 π electrons. They therefore satisfy the Hückel rule for aromaticity.[4] The bonds in these molecules exhibit substantial ellipticities, and in each case the major axis of the ellipticity, the axis of the soft curvature λ_2, is directed perpendicular to the plane of the ring. This is the charge density analogue of a molecule with a delocalized π system. The delocaliziation is most pronounced in S_2N_2. This is illustrated in Figure 5, which displays contours of $\nabla^2\rho$ in the diagonal planes containing two sulfur or two nitrogen nuclei. In S_4^{2+} (Figure 5a) the region of charge concentration associated with the nonbonded maximum on sulfur (the lone pair of the Lewis model) is extended over the sulfur atoms, resulting in significant charge concentrations above and below the plane of the nuclei. The out-of-plane concentrations on sulfur are more pronounced in S_2N_2 (Figure 5b). In this case the single nonbonded maximum in $-\nabla^2\rho$ has bifurcated into two. In terms of the orbital model this can be viewed as a result of the "back-polarization of π density" from N to S.

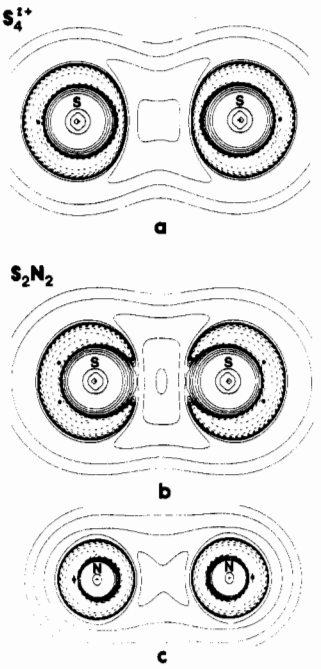

Figure 5. Contour maps of $\nabla^2\rho$ for planes perpendicular to the plane of the nuclei along an SS diagonal in S_4^{2+} (a) and along SS (b) and NN (c) diagonals in S_2N_2. The positions of the nonbonded maxima in the valence shell charge concentrations are indicated by dots. The values of $\nabla^2\rho$ at these positions are −0.43 au in S_4^{2+} and −0.52 au on S and −2.12 au on N in S_2N_2.

In addition to the nonbonded charge concentration present on each atom in these two molecules, each sulfur atom possesses two regions of charge depletion (see Figure 4a, b). The associated critical points in $\nabla^2\rho$ determine the positions of maximum charge depletion in the valence shells of the sulfur atoms. These positions locate the sites of nucleophilic attack and the preferred points of interaction with a counterion or base in a crystal structure.[10] Passmore et al.[21] have reported the crystal structure of $S_4(AsF_6)_2 \cdot 0.6SO_2$. The shortest anion–cation contacts in this crystal (2.67–2.76 Å) are those resulting from the in-plane bridging of each S–S bond in the cation by a fluorine atom of the anion. Such bridging is anticipated by the Laplacian of ρ for S_4^{2+}. A critical point denoting a center of charge depletion in the valence shell of a sulfur atom lies in the plane of the nuclei and forms an angle of 60.1° with the adjacent S–S bond. Since the angle is acute, a single fluorine atom may bridge each pair of such critical points on neighboring sulfur atoms, in the manner indicated by the arrows in Figure 4a. The average experimental value of the FSS angle in the bridged structure is 68° as determined by the contact distance of the F atom.

The properties of the Laplacian of ρ for S_4N_4 correlate with one particular Lewis structure for this molecule. A normal doubly coordinated sulfur atom as in H_2S, for example, exhibits two bonded charge concentrations whose maxima subtend an angle of 95° with the S nucleus and two broader, nonbonded charge concentrations in the perpendicular plane subtending an angle of 134°.[10] In N_4S_4 the S atom bears a net charge of 1.29+ (compared to 0.34+ in H_2S) and one of the nonbonded charge maxima has been transformed into a bonded maximum, forming a long S–S bond of the closed-shell type. In addition each sulfur possesses two bonded maxima linking the N atoms subtending an angle of 101.5°. The angle between these bonded and single nonbonded charge concentration on sulfur is 122.8°, while the angle between

(21) Passmore, J.; Sutherland, G.; White, P. S. *J. Chem. Soc., Chem. Commun.* **1980**, 330.

the nonbonded and the S–S bonded charge concentrations is only 106.8°. This is in accord with VSEPR model[20] since the bonded charge concentration of the long, weak S–S bond should occupy less space than the S–N bonded charge concentrations. It is observed here that each nitrogen nucleus serves as a terminus for only two bond paths, and in confirmation of this property of the gradient vector field of ρ, the Laplacian of ρ for a nitrogen atom exhibits just two equivalent bonded charge concentrations. One possible resonance structure for N_4S_4 has alternating single and double S–N bonds and a single lone pair on each nitrogen. However, each nitrogen atom in N_4S_4 is found to exhibit two equivalent nonbonded concentrations of charge contrary to the above resonance structure. Thus in terms of the net charges on the atoms, the network of bonds, and the number and location of the bonded and nonbonded charge concentrations—*all as determined by the properties of its charge distribution*—the N_4S_4 molecule is best represented by Lewis structure A.

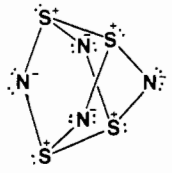

A

The positions of the bonded maxima on nitrogen subtend an angle of 112° compared to the bond angle of 117°. The value of $\nabla^2\rho$ at these maxima is −0.76 au, compared to the value of −1.13 au for the corresponding maxima in S_2N_2. The two equivalent nonbonded charge concentrations subtend an angle of 92° at the nitrogen nucleus, and each subtends an angle of 107° with the nearest bonded charge maximum. The value of $\nabla^2\rho$ at a nonbonded charge maximum on nitrogen, the primary center for electrophilic attack, is −1.65 au. The nonbonded charge concentrations on nitrogen are displaced above and below the plane of the nitrogen nuclei by ~30°. The relative orientations of the valence charge concentrations on N in N_4S_4 are indicated in B.

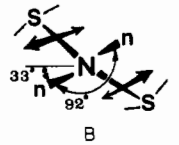

B

The value of the ellipticity for an S–N bond in S_4N_4 (at both the STO-3G and 6-21G* levels of calculation), while less than the values for the delocalized systems discussed above, indicates that the distribution of charge of an S–N bond in this molecule is preferentially disposed in a particular plane to a significant degree. The major axis of this ellipticity is approximately perpendicular to the plane formed by the three nuclei in a

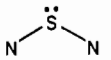

fragment. This ellipticity could be the result of the partial delocalization of a nonbonded charge concentration on nitrogen, as each such concentration is closely aligned with the major axis of its nearest S–N bond. This would also account for the angle between the nonbonded charge concentrations on nitrogen being less than expected on the basis of the VSEPR model (see B). The site of nucleophilic attack on N_4S_4 should be on the sulfur atom. There are two sites of charge depletion in the valence shell of each sulfur atom. They are nearly in the plane of the

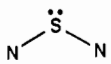

fragment and form an angle of 59° with the S–N bond axes. The value of $\nabla^2\rho$ at the critical point is +0.02 au.

Registry No. S_2N_2, 25474-92-4; S_4^{2+}, 12597-09-0; $S_4N_4^{2+}$, 64006-48-0; S_4N_4, 28950-34-7; H_2S_2, 13465-07-1; $S_6N_4^{2+}$, 53518-36-8; S_8, 10544-50-0; S_8^{2+}, 11062-34-3; S_8^{4+}, 96411-99-3; N, 7727-37-9; S, 7704-34-9.

Contribution from the Department of Chemistry,
New Mexico State University, Las Cruces, New Mexico 88003

Kinetic Aspects of the Iron(III)–Tetrakis(*p*-sulfonatophenyl)porphine System

A. A. EL-AWADY, P. C. WILKINS, and R. G. WILKINS*

Received January 11, 1985

The kinetics of dimerization of $Fe(TPPS)(H_2O)^{3-}$ to $(TPPS)Fe–O–Fe(TPPS)^{8-}$ (TPPS = tetrakis(*p*-sulfonatophenyl)porphine) have been studied by pH jump–stopped flow at I = 0.1 M ($NaNO_3$) and 25 °C. The spectral characteristics of the intermediate $Fe(TPPS)(OH)^{4-}$ were obtained by rapid-scan experiments. Spectral–pH measurements allow the determination of the pK_a of $Fe(TPPS)(H_2O)^{3-}$ as 7.0 ± 0.2. The variation of the second-order dimerization rate constant (k_{obsd}) with pH (6.5–9.2) is given by $k_{obsd} = kK_a[H^+]^{-1}[1 + K_a[H^+]^{-1}]^{-2}$. This is consistent with a mechanism in which $Fe(TPPS)(H_2O)^{3-}$ and $Fe(TPPS)(OH)^{4-}$ are the important reactant pair ($k = 1.5 \times 10^6$ M^{-1} s^{-1}). The breakdown of dimer into monomer was measured by pH-drop and dithionite reduction experiments. The first-order rate constants k_{obsd} obeyed the expression $k_{obsd} = k[H^+](K_a + [H^+])^{-1}$. This was consistent with a mechanism in which a protonated dimer (pK_a = 6.4) rapidly dissociates (k = 8.0 s^{-1}). Spectral evidence for the protonated dimer was obtained by rapid scan. The combination of rate with pK_a data gives an overall equilibrium constant which is in excellent agreement with that determined directly.

Introduction

Metalloprophyrins are important examples of macrocyclic complexes and have been extensively examined from every viewpoint.[1] The study of the properties of iron porphyrin complexes, for example, is important in reaching an understanding of the role and function of a wide variety of biological materials, in which an iron–porphyrin core plays a vital role.[2] There are however a limited number of water-soluble metalloporphyrins forming well-behaved nonaggregated species in aqueous solution. The iron(III)–tetrakis(*p*-sulfonatophenyl)porphine (abbreviated TPPS) system appears to be such an example. Originally examined by Fleischer et al.,[3] the conditions for the formation of a iron(III) monomer and an oxo-bridged iron(III) dimer have been well established:

$$2Fe(TPPS)(OH_2)^{3-} \rightleftharpoons (TPPS)Fe–O–Fe(TPPS)^{8-} + H_2O + 2H^+ \quad K_1 \quad (1)$$

(1) Smith, K. M., Ed. "Porphyrins and Metalloporphyrins"; Elsevier: Amsterdam, 1975. Dolphin, D., Ed. "The Porphyrins"; Academic Press: New York, 1978.
(2) Lever, A. B. P., Gray, H. B., Eds. "Iron Porphyrins"; Addison-Wesley: Reading, MA, 1983.
(3) Fleischer, E. B.; Palmer, J. M.; Srivastava, T. S.; Chatterjee, A. *J. Am. Chem. Soc.* **1971**, *93*, 3162.

0020-1669/85/1324-2053$01.50/0